Chapter 13
Nonlinear Finite Element and Atomistic Modelling of Dislocations in Heterostructures

Paweł Dłużewski, Toby D. Young, George P. Dimitrakopulos, Joseph Kioseoglou, and Philomela Komninou

Abstract. A continuum and atomistic approach to the modelling of dislocations observed by the High Resolution Transmission Electron Microscopy (HRTEM) is discussed. We present a methodology for the analysis of dislocations, stacking faults and interfacial regions in crystal heterostructures by using experimental measurements, and atomistic/continuum models. The derived method is capable of handling dense arrays of dislocations as well as large areas of the interface between two crystal structures. As an example, we consider stacking faults in bulk GaN and a misfit dislocation network in a GaN/sapphire interfacial region through relaxation of strain and associated residual stresses; where the quantification of the latter is beyond the reach of experiment alone.

13.1 Introduction

This chapter achieves a reciprocal relation between atomistic and continuum models of the extended crystal defects observed in semiconductor structures. In particular, a focus is applied to regions containing dislocations and/or stacking faults in bulk crystals, and to misfit dislocation networks in the interfacial region of a film/substrate heterostructure. The connection between the continuum and atomistic models is divided into two parts and illustrated by following two examples:

(a) The atomistic models of dislocations, typically found in semiconductor materials, are constructed by means of a set of equations that describe the distortion

Paweł Dłużewski and Toby D. Young
Institute of Fundamental Technological Research PAS, ul. Pawińskiego 5 B, 02-106 Warsaw, Poland
e-mail: pdluzew@ippt.gov.pl and tyoung@ippt.gov.pl

George P. Dimitrakopulos, Joseph Kioseoglou and Philomela Komninou
Department of Physics, Aristotle University of Thessaloniki, GR-54124 Thessaloniki, Greece
e-mail: gdim@auth.gr, sifisl@auth.gr, komnhnoy@auth.gr

M. Kuczma, K. Wilmanski (Eds.): Computer Methods in Mechanics, ASM 1, pp. 239–253.
springerlink.com

field of the straight–mixed dislocation introduced by a slip/climb plane (stacking fault) to the crystal lattice. Such partial dislocations and stacking faults as observed on HRTEM images are discussed in this chapter.

(b) The misfit dislocations arising at a planar heterojunction formed between semiconductor film and substrate are reconstructed in the atomistic and 3D finite element models by taking advantage of experimentally obtained strain maps.

In order to assure the fulfillment of a proper reciprocal relation between the continuous and discrete configurations of these systems, the theoretical predictions are referred back to observations obtained by experiment. From this, it may then be possible to investigate such a system in terms of its effectiveness in technological applications and devices.

In particular, as a practical implementation of this scheme, we analyse structural defects introduced by the mismatch between GaN and sapphire lattices in three conjoined steps of modelling. In the first step the reconstruction of the lattice distortion fields was performed starting from observations of the GaN/sapphire interface by HRTEM. Having as input the experimental values of the lattice constants, 3D crystallographic models of the stacking faults and interface were constructed. Geometrical Phase Analysis [10] was then applied to the experimental and the corresponding simulated images in order to obtain initial lattice displacement and strain fields in the interfacial region. This data was taken as input for Finite Element Analysis (FEA) thereby overcoming the obstacle of a lack of empirical potentials suitable for describing heterostructures within molecular dynamics simulations. The 3D model, corresponding to a few parallel misfit dislocations in the HRTEM image, was constructed with a fundamental motif structure and multiplied in such a way as to obtain a sample of reasonable size with a number of dislocation nodes trapped inside thus forming a complex network of misfit dislocations.

The remainder of this chapter is organised as follows: In section 13.2, the mathematical foundations of the nonlinear continuum theory are discussed and mutual tensor relations between the lattice and plastic distortions, Burgers vector and elastic-plastic deformation tensors are discussed. Section 13.3 is devoted to dislocations and stacking faults reconstructed in the bulk crystals. Section 13.4 is devoted to the HRTEM analysis and reconstruction of the misfit dislocation net in the interfacial region of henerostructure GaN/Al_2O_3. In that section, we apply our method for reconstructing 3D source distortion maps from 2D and consider the relaxation process of the strain energy of the heterostructure by a discrete space formalism within FEA. Conclusions are drawn in Section 13.5.

13.2 Continuum Theory of Discrete Dislocations

In the linear theory of dislocations the gradient of crystal deformation is decomposed additively into the lattice and plastic distortion tensors, according to

$$\operatorname{grad}\mathbf{u}_{\mathrm{tot}} = \boldsymbol{\beta} + \boldsymbol{\beta}_{\mathrm{pl}}\,, \tag{13.1}$$

cf. [16]. By assumption, the lattice distortion $\boldsymbol{\beta}$ is composed of the antisymmetric tensor of crystal lattice rotation and symmetric tensor of elastic strain, respectively

$$\boldsymbol{\beta} = \mathbf{w} + \boldsymbol{\varepsilon}\,. \tag{13.2}$$

The plastic distortion $\boldsymbol{\beta}_{\mathrm{pl}}$ is identified with an asymmetric strain tensor being isoclinic with the lattice rotation. This nomenclature comes from the theory of elastoplastic Cosserat continua where the particle rotation $\boldsymbol{\chi}$ and elastic/plastic strains are identified respectively with: $\boldsymbol{\chi} \equiv \mathbf{w}$, $\boldsymbol{\varepsilon} \equiv \boldsymbol{\varepsilon}$ and $\boldsymbol{\varepsilon}_{\mathrm{pl}} \equiv \boldsymbol{\beta}_{\mathrm{pl}}$; which gives

$$\operatorname{grad}\mathbf{u}_{\mathrm{tot}} = \boldsymbol{\chi} + \boldsymbol{\varepsilon} + \boldsymbol{\varepsilon}_{\mathrm{pl}}\,. \tag{13.3}$$

where the elastic strain tensor $\boldsymbol{\varepsilon}$ is no longer symmetric. Contrary to the Cosserat continua, in the continuum theory of dislocations it is assumed that the material particle cannot rotate independently of the displacement field, and therefore a simplified notation gathering together the elastic strain and crystal lattice rotation into a common lattice distortion tensor $\boldsymbol{\beta}$ is more convenient.

13.2.1 Burgers Vector

According to the state–of–the–art of the nonlinear continuum theory of dislocations, the total deformation gradient can be decomposed multiplicatively into elastic and plastic deformation parts and rewritten in the form

$$\mathbf{F}_{\mathrm{tot}} = \mathbf{F}\,\mathbf{F}_{\mathrm{pl}}\,. \tag{13.4}$$

The integration of lattice distortions over Burgers circuits gives

$$\mathbf{b} = \oint_{\mathrm{c}} d\mathbf{x} = \oint_{\mathrm{O}} \mathbf{F}\, d\widehat{\mathbf{x}} = \oint_{\mathrm{c}} (\mathbf{1} + \widehat{\boldsymbol{\beta}})\, d\widehat{\mathbf{x}}\,, \tag{13.5a}$$

$$-\widehat{\mathbf{b}} = \oint_{\mathrm{C}} d\widehat{\mathbf{x}} = \oint_{\mathrm{o}} \mathbf{F}^{-1} d\mathbf{x} = \oint_{\mathrm{o}} (\mathbf{1} - \boldsymbol{\beta})\, d\mathbf{x}\,, \tag{13.5b}$$

where $\mathbf{1}$, $\mathbf{b}$ and $\widehat{\mathbf{b}}$ are the metric tensor of the Euclidean space, and the spatial and true Burgers vectors, respectively. The symbols $\mathrm{c}, \mathrm{C}, \mathrm{o}, \mathrm{O}$ denote the open and closed Burgers circuits situated respectively in the current (Eulerian) and reference (intermediate) configurations. It is worth emphasising here that the lattice distortion $\boldsymbol{\beta}$ is related to lattice spacings in the current configuration. Alternatively, the distortions can be referred back to the spacings in a perfect lattice, which gives the following reversible transformation rule

$$\widehat{\boldsymbol{\beta}} = (\mathbf{1} - \boldsymbol{\beta})^{-1} - \mathbf{1}\,. \tag{13.6}$$

Usually, in the linear theory the difference between differentiation over the current, reference and intermediate configurations are neglected, i.e. it is assumed that $\frac{\partial \mathbf{u}}{\partial \mathbf{x}} \approx \frac{\partial \mathbf{u}}{\partial \mathbf{x}}, \widehat{\boldsymbol{\beta}} \approx \boldsymbol{\beta}$, $\mathrm{O} \equiv o$, etc. Given such a simplified approach, the differential equation sets obtained reduce to linear sets, and thanks to analytical methods available for linear systems many very useful analytical formulae have be derived for dislocations.

13.2.2 Analytical Equations for Mixed Straight Dislocation

The total displacement field around a mixed straight-line dislocation in an isotropic elastic material is defined by the classical formulae coming back to works by [19] and [23]. Here the equations are written in a more general form as

$$\begin{aligned} u_x &= \frac{b_x}{2\pi}\Big(\arctan\frac{y}{x} + \frac{xy}{2(1-\nu)(x^2+y^2)}\Big) - b_x H\big(\arctan\frac{y}{x} - \varphi\big), \\ u_y &= -\frac{b_x}{2\pi}\left(\frac{1-2\nu}{4(1-\nu)}\ln(x^2+y^2) + \frac{x^2-y^2}{4(1-\nu)(x^2+y^2)}\right), \\ u_z &= \frac{b_z}{2\pi}\arctan\frac{y}{x} - \frac{b_z}{2}. \end{aligned} \tag{13.7}$$

where the edge and screw components of the Burgers vector, b_x and b_z, are parallel to the x and z axes respectively. The symbol φ denotes the angle composed by edge component of the Burgers vector with the crystal plane the partial dislocation is introduced into the crystal; the Heaviside step function $H(x)$ is defined according to the following convention: $H(x) = 1$ for $x \geq 0$, and $H(x) = 0$ for $x < 0$. For partial dislocations the plane mentioned above can be identified with a stacking fault plane, see Fig. 13.1.

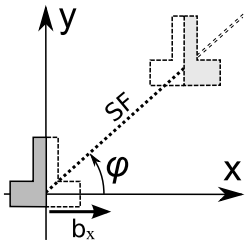

Fig. 13.1 Partial dislocation bounding a stacking fault.

Non–vanishing components of lattice distortions are

$$\begin{aligned} \beta_{xx} &= \frac{-b_x}{2\pi}\,\frac{(3-2\nu)x^2y + (1-2\nu)y^3}{2(1-\nu)(x^2+y^2)^2}, & \beta_{xy} &= \frac{b_x}{2\pi}\,\frac{(3-2\nu)x^3 + (1-2\nu)xy^2}{2(1-\nu)(x^2+y^2)^2}, \\ \beta_{yx} &= \frac{-b_x}{2\pi}\,\frac{(1-2\nu)x^3 + (3-2\nu)xy^2}{2(1-\nu)(x^2+y^2)^2}, & \beta_{yy} &= \frac{b_x}{2\pi}\,\frac{(1+2\nu)x^2y - (1-2\nu)y^3}{2(1-\nu)(x^2+y^2)^2}, \\ \beta_{zx} &= \frac{-b_z}{2\pi}\,\frac{y}{x^2+y^2}, & \beta_{zy} &= \frac{b_z}{2\pi}\,\frac{x}{x^2+y^2}, \end{aligned} \tag{13.8}$$

It is worth emphasizing that (13.7) does not describe the total displacement field but only its elastic part in a *singly connected* domain $\arctan\frac{y}{x} \neq \varphi$. The plastic

distortions can be recovered here from the compatibility condition, $\oint_o d\mathbf{u}_{tot} = 0$, which gives

$$\beta_{\mathrm{pl}xx} = \frac{x}{x^2+y^2}\,\delta\left(\arctan\frac{y}{x} - \varphi\right), \qquad \beta_{\mathrm{pl}xy} = -\frac{y}{x^2+y^2}\,\delta\left(\arctan\frac{y}{x} - \varphi\right), \tag{13.9}$$

where $\delta(\cdot)$ denotes the Dirac delta function.

13.3 Atomistic Reconstruction of Dislocations

In many cases the analytical solutions obtained by means of the linear theory of dislocations are used to generate the input files for atomistic modelling of the physical properties of dislocation cores. In case of the wurtzite structure of GaN such a method has been used in many papers starting from [1]. The structure of such obtained cores depends on which position the dislocation center has taken in the reference unit crystal cell as shown in figure 13.2.

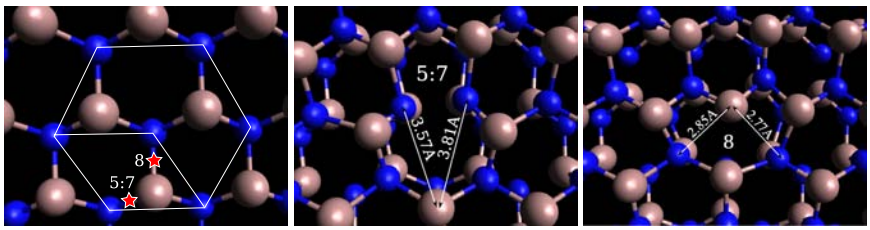

Fig. 13.2 Dislocation core structures generated by means of (13.7) for $\mathbf{b} = \frac{1}{3}\langle 2\bar{1}\bar{1}0\rangle$ in GaN, on the left: the reference unit cell with depicted positions of dislocation centers assumed to generate the 5:7 and 8-atom ring cores shown on the right, respectively.

The dislocation cores generated by the use of (13.7) do not hold symmetry of atomic bonds distribution. To avoid the asymmetry some modification into (13.7) was considered by [3], cf. [20]. Nevertheless, to obtain a symmetric distribution we should apply finite deformation theory in which the difference between differentiation over the reference and spatial configurations are taken into account. The problem is that the strict analytical solutions based on the nonlinear theory have not been obtained for most of the typical problems of the dislocation theory as yet.

13.3.1 HRTEM Investigations of Partial Dislocations in GaN

GaN-based wide band-gap semiconductor technology has offered important device applications in optoelectronic and high power-frequency-temperature microelectronics. Extensive studies of dislocation core structures are being performed in

order to assess their influence on a number of material properties and phenomena, e.g. [21, 2, 26, 18, 17, 8]. We have recently derived the core structures of the Shockley partial dislocations that delimit the I_1 type of intrinsic stacking fault [12] which is a low energy fault of frequent occurrence. These defects can be constructed from a perfect crystal by removal or addition a disc of atoms in the (0001) basal plane (vacancy or interstitial disc) followed by a shear.

Assuming that the line direction of the partial dislocation is along $[1\overline{2}10]$, the dislocation may exhibit either the edge or mixed character. Let xz be the (0001) plane, with z along the dislocation line (i.e. $[1\overline{2}10]$) and x along $[10\overline{1}0]$. Consequently, the y axis is along $[0001]$. In the case of edge-type partials $\mathbf{b}_{edge} = \mathbf{b}_x + \mathbf{b}_y$ where $\mathbf{b}_x = \pm\frac{1}{3}[10\overline{1}0]$ and $\mathbf{b}_y = \pm\frac{1}{2}[0001]$. In the case of mixed-type partials, $\mathbf{b}_{mixed}$ can be decomposed into a screw $\mathbf{b}_z = \frac{1}{6}[1\overline{2}10]$ component and two edge components, $\mathbf{b}_x = \pm\frac{1}{6}[10\overline{1}0]$ and $\mathbf{b}_y = \pm\frac{1}{2}[0001]$. Using an empirical interatomic potential, 6 stable configurations for each of 4 variants of Shockley partials, $\frac{1}{6}[20\overline{2}3]$, $\frac{1}{6}[20\overline{23}]$, $\frac{1}{6}[2\overline{2}03]$, $\frac{1}{6}[2\overline{2}0\overline{3}]$, have been obtained, and their energies and atomic configurations were given by [12]. A $\frac{5}{7}$-atom ring core in which the atoms are tetrahedrally coordinated was found energetically favourable among the edge partial dislocation configurations. The $\frac{5}{7}$ and 12 atom rings were obtained as low energy cores for the mixed-type partials of the a and b cases, respectively, although none of these was found to comprise only tetrahedrally coordinated atoms.

The HRTEM observations of edge and mixed $\frac{1}{6}\langle 20\overline{2}3\rangle$ partial dislocations in GaN have also been presented previously. Through GPA of strain fields, as well as peak finding on white dots, comparison between experimental images and simulated images of relaxed structures was performed. The $\frac{5}{7}$ or 12-atom rings were clearly identified for the experimental image of figure 13.3a and an 8-atom ring was identified for the HRTEM image of figure 13.3b [14]. For the mixed partial dislocation of figure 13.3c, the peak-finding analysis has indicated the 12- or 10-atom rings [11].

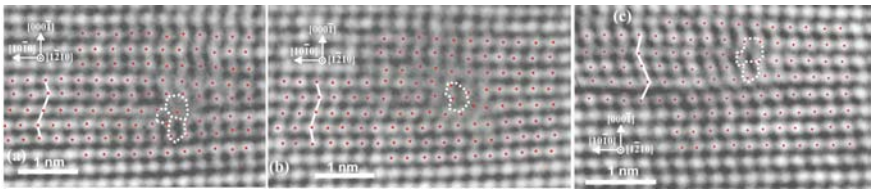

Fig. 13.3 HRTEM images of edge partial dislocations $\frac{1}{6}[20\overline{2}3]$ bounding a stacking fault I_1. The intensity peaks corresponding to the positions of atomic columns have been marked with red dots, the atom rings has been identified by both GPA and peak finding [13].

13.4 Misfit Dislocations in Heterostructure GaN/Al_2O_3

HRTEM provides a suitable method with which to quantitatively probe the details of lattice displacements with sub–angstrom accuracy [9]. The HRTEM simulated images of the interface model were generated using the multi–slice algorithm [25] of the EMS software. Prior to comparison with the simulations, the experimental conditions of thickness and defocus were determined by calculating the map of through focus thickness images of perfect GaN. In the HRTEM micrograph of figure 13.4a the GaN/Al_2O_3 interface is depicted along the $[11\bar{2}0]$ (GaN) and $[10\bar{1}0]$ (Al_2O_3) directions. Using Fourier filtering it is possible to visualise the edge component of one set of misfit dislocations as terminating fringes of the corresponding substrate lattice planes; figures 13.4b and 13.4c.

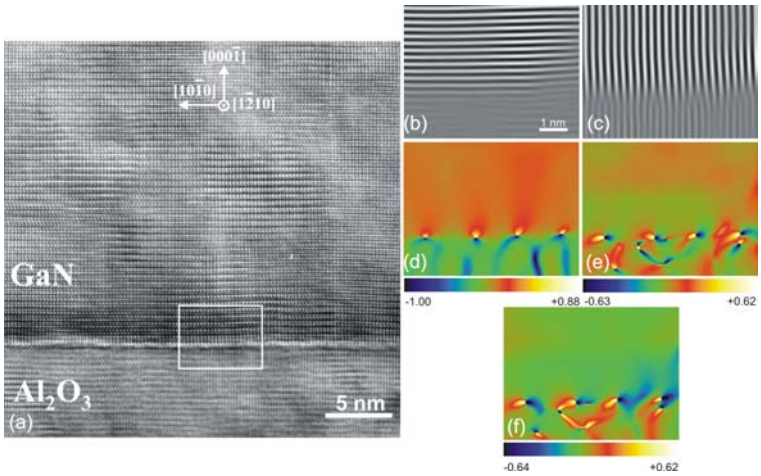

Fig. 13.4 In the left panel (a) HRTEM micrograph of the film/substrate system. In the right panel, measurements taken from the white bounding box in (a) are the Bragg images from Fourier filtering along (b) [0002] and (c) $[10\bar{1}0]$; and images of lattice distortions (d) ε_{xx}, (e) ε_{xy} and (f) w_{xy} (thickness=2.2nm, defocus=59nm and white spots represent the atomic columns projection along $[1\bar{2}10]$).

13.4.1 Crystallographic Model

The $[10\bar{1}0]$ d-spacing of GaN was determined experimentally from figure 13.4a to be $d = 2.725$Å yielding a lattice parameter $a = 3.1466$Å. By assuming pure bi-axial strain, and with the use of the elastic constants C_{13} and C_{33}, the lattice c parameter was calculated to be $c_{cal} = 5.2025$Å. The same parameter was determined experimentally to be $c_{exp} = 5.19$Å. From the difference between c_{cal} and c_{exp} it is clear

that in addition to bi–axial strain the GaN film also exhibits hydrostatic or uniaxial strain.

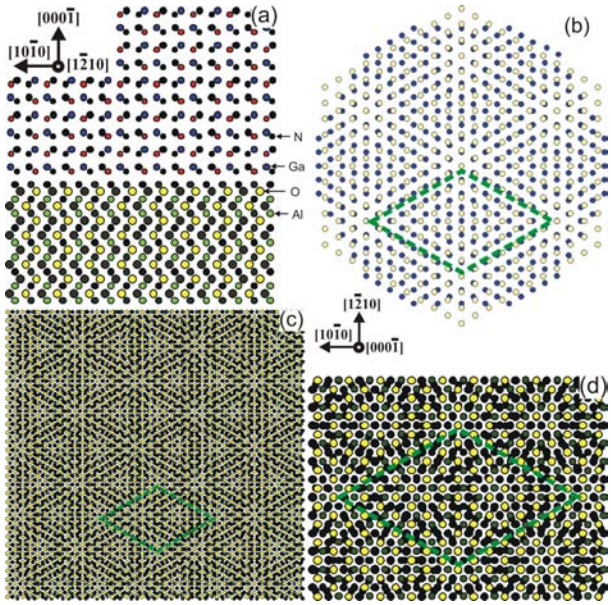

Fig. 13.5 (a) Schematic illustration along $[1\bar{2}10]$ GaN/Al_2O_3 heterostructure. (b) Plan-view along [0001] of two relatively rotated by $\pi/6$ hexagonal lattices showing the translation periodicity at the interface (dichromatic pattern). (c) Plan view along [0001] of the relatively rotated crystal structures (wurtzite GaN and Al_2O_3) thus forming a dichromatic complex [22]. The translation periodicity and moiré pattern are shown as well as the trigonal-hexagonal primitive unit-cell employed here. (d) Enlarged view of the primitive unit-cell. Large and small circles denote distinct atomic species, shading of atoms denote levels along the projection direction.

The lattice mismatch between crystal layers is defined by the simple relation $f = (a_{epi} - a_{ref})/a_{ref}$; where a_{epi} and a_{ref} denote the epitaxial and reference lattice constants respectively. Taking GaN as reference the lattice mismatch was calculated to be $f = 0.5124$, and $f = 0.3388$ was found by the use of Al_2O_3 as a reference. A lateral rotation of $\pi/6$ radians of the GaN basal plane significantly reduces the lattice mismatch to $f = 0.1268$ with GaN as the reference and $f = 0.1452$ with Al_2O_3 as the reference. The latter configuration is investigated here. Figure 13.5a illustrates the crystallographic model of the bi–crystal along $[1\bar{2}10]$ (*i.e.* the same projection direction as figure 13.4a).

A 3D atomic configuration of the interface was duly constructed using crystallographic data and HRTEM image simulations were calculated. GPA was then applied to the simulated images in order to obtain the displacement and strain fields in the interface region. This data was used as input for FEA [15, 6].

In figures 13.5b and 13.5c the unit–cell is enlarged. In figure 13.5d the coincident translational periodicity and primitive unit-cell are illustrated. The bi-crystal layer group is $p3$. Each unit-cell contains one dislocation; thereby its symmetry is reduced to pl and there are three possible variants of $2\pi/3$ radians (*i.e.* the co–set decomposition $\{p3\} = \{pl\} \cup 3^{+}\{pl\} \cup 3^{-}\{pl\}$).

Figure 13.6 illustrates schematically the unit cell given in figures 13.5c and 13.5d. Rotation around the point of symmetry (black closed triangles) of the sub-cell (dash-dot green lines) in figure 13.6a give rise variations of the primitive unit-cell (solid blue lines). The unit-cell is sequentially translated by the coincidence periodicity to obtain a honeycomb network of misfit dislocations crossing at $2\pi/3$ radians depicted in figure 13.6b. The full structure is then taken into FEA described in Section 13.4.2.

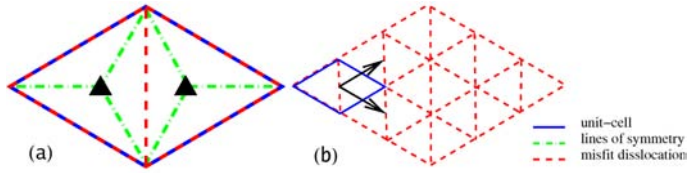

Fig. 13.6 Schematic representation of (a) co-set decomposition of the primitive unit-cell employed here (*c.f.* figure 13.5c) and (b) construction of the resultant initial honeycomb misfit dislocation pattern through translation of the primitive unit-cell by the coincidence periodicity. Solid blue lines give the boundary of a unit-cell and dashed red lines denote misfit dislocations. The green dash-dot lines mark out boundaries of the sub-cells with point rotational symmetry.

13.4.2 Finite Element Modelling of Misfit Dislocations

Linear elasticity predicts equal volumes of compressed and extended regions around dislocations while experimental evidence shows that extended regions occupy a larger volume than compressed regions [24]. This asymmetry is widely assumed to be quantified by the third-order elastic constants which play a crucial rôle in the elastic behaviour of real crystal structures. In the last decade a number of differing methods based on a theory of linear elasticity have been employed for the simulation and analysis of lattice dislocations. In this chapter a different approach is used that has emerged in more recent years and is based on a theory of nonlinear elasticity [6, 4]. In this way we aim to properly take into account the nonlinear elastic behaviour observed by experiment.

We distinguish between three principal components that together contribute to the total deformation of the system. First, the source deformation field assumed to determine the lattice distortion field for the entire heterostructure; secondly, a chemical deformation gradient describing the transition between perfect lattices of

Al_2O_3 and GaN; and thirdly, the source deformation gradient determined by GPA in relation to some region of Al_2O_3 chosen to be the reference region to measure the deformation map for the whole structure visible on the HRTEM image.

The total deformation gradient $\mathbf{F}$ is decomposed therefore into three components:

$$\mathbf{F}_{\text{tot}} = \mathbf{F}\,\mathbf{F}_{\text{ch}}\mathbf{F}_{\circ}^{-1}\,, \tag{13.10}$$

where $\mathbf{F}$, $\mathbf{F}_{\text{ch}}$ and $\mathbf{F}_{\circ}$ are the elastic, chemical and lattice deformation gradient, respectively. The last gradient is extracted from the HRTEM image by computer image processing, cf. [6]. Alternatively, the gradient can be generated by using the analytical formulae of the continuum theory of dislocations, see [7]. The chemical deformation tensor in Al_2O_3 region is assumed to be the unit tensor of the Euclidean space. In the GaN and transit regions it was assumed that

$$F_{\text{ch}} = \begin{bmatrix} \dfrac{a_{\text{GaN}}}{a_{\text{Al}_2\text{O}_3}} & 0 & 0 \\ 0 & \dfrac{a_{\text{GaN}}}{a_{\text{Al}_2\text{O}_3}} & 0 \\ 0 & 0 & \dfrac{c_{\text{GaN}}}{c_{\text{Al}_2\text{O}_3}} \end{bmatrix} n(\mathbf{x}) \tag{13.11}$$

where $n(\mathbf{x})$ is the molar fraction of GaN spanned on eight corner nodes of elements situated in the transit FE layer. The source deformation and distortion tensors extracted from HRTEM image satisfy the following relation

$$\mathbf{F}_{\circ}^{-1} = \mathbf{1} - \boldsymbol{\beta}_{\circ}\,. \tag{13.12}$$

The continuum model used here is based on the integration of the equilibrium condition on the Cauchy stress tensor,

$$\operatorname{div}\boldsymbol{\sigma} = 0\,, \tag{13.13}$$

In terms finite strains, where the stress measure conjugate by work with the logarithmic strain is referred to the undeformed (perfect) crystal lattice and satisfies the following linear constitutive equation

$$\widehat{\boldsymbol{\sigma}} = \widehat{\mathbf{c}}\,\widehat{:}\,\widehat{\boldsymbol{\varepsilon}}\,, \tag{13.14}$$

where a hat denotes quantities in the reference lattice configuration. Here $\widehat{\boldsymbol{\varepsilon}}$ is the Lagrangian logarithmic strain tensor defined as $\widehat{\boldsymbol{\varepsilon}} = \ln\mathbf{U}$, where $\mathbf{U}$ is the right stretch tensor of elastic deformation from the polar decomposition $\mathbf{F} = \mathbf{R}\mathbf{U}$, where $\mathbf{R}$ is the orthogonal tensor of rotation. The fourth–order proper–symmetric tensor of elastic stiffness $\widehat{\mathbf{c}}$ is assumed here to be a tensor of material constants.

Due to nonlinear geometric changes between the reference and current lattice configurations, it can be shown that such constitutive equation leads to a nonlinear relation for the Cauchy stress

$$\boldsymbol{\sigma} = \mathbf{c} : \boldsymbol{\varepsilon}, \tag{13.15}$$

where

$$\boldsymbol{\varepsilon} = \mathbb{A}^{-T} : \widehat{\boldsymbol{\varepsilon}}, \qquad \mathbf{c} = \mathbb{A} : \widehat{\mathbf{c}} : \mathbb{A}^{T} \det \mathbf{F}^{-1}, \tag{13.16}$$

where $\mathbb{A}^{ij}{}_{IJ} = R^{i}{}_{K} R^{j}{}_{L} \widehat{\mathbb{A}}^{KL}{}_{IJ}$. The geometric meaning of the fourth–order proper–symmetric tensor $\widehat{\mathbf{A}}$ as an isotropic tensor function of $\widehat{\boldsymbol{\varepsilon}}$ is discussed in [4].

Using the virtual work principle the following nonlinear matrix equation is found

$$\mathbf{P}(\mathbf{a}) = \mathbf{f}, \tag{13.17}$$

where the vector $\mathbf{P}$ is a nonlinear function of nodal variables $\mathbf{a}$, i.e.

$$\mathbf{P} = \int_{v} grad^{T} \mathbf{W} \boldsymbol{\sigma} \, d\mathbf{v}, \qquad \mathbf{a} = \begin{bmatrix} \mathbf{u} \\ n \\ \widehat{\boldsymbol{\beta}}_{\circ} \end{bmatrix}, \qquad \mathbf{f} = \int_{\partial \mathbf{v}} \mathbf{W} \boldsymbol{\sigma} \, d\mathbf{s}. \tag{13.18}$$

and $\widehat{\boldsymbol{\beta}}_{\circ} = (\mathbf{1} - \boldsymbol{\beta}_{\circ})^{-1} - \mathbf{1}$. $\mathbf{W}$ denotes the weighting function determined in relation to the current (iterated) configuration. Using the Newton–Raphson method, the non-symmetric equation set (13.17) was solved for displacements under the fixed fields $\widehat{\boldsymbol{\beta}}_{\circ}$ and n.

The components of distortion were cropped to represent the periodicity of parallel misfit dislocations on the interface and rescaled to a resolution of 9×11 pixels. The strain value at each pixel represented by a single corner node of the 27-node Lagrangian element [4, 5]. For an extension from the 2D mapping of figure 13.4 to a 3D continuum model of the strain energy similar operations are applied on the distortion tensor β as as were applied on the spatial coordinate system as described in subsection 13.4.1. For a single misfit dislocation the reconstruction of missing 3D source distortion components from 2D HRTEM images, cf. figure 13.5, was done by using the following relation [6]

$$\widehat{\boldsymbol{\beta}}_{\circ} = \begin{bmatrix} \widehat{\beta}_{\circ xx} & 0 & \widehat{\beta}_{\circ xz} \\ \frac{\sqrt{2}}{2} \widehat{\beta}_{\circ xz} & 0 & \frac{\sqrt{2}}{2} \widehat{\beta}_{\circ zz} \\ \widehat{\beta}_{\circ zx} & 0 & \widehat{\beta}_{\circ zz} \end{bmatrix}. \tag{13.19}$$

13.4.3 Reconstruction of 3D Structure into FEA

The GaN/Al_2O_3 system FEA in the resultant configuration of relaxed strain is given in figure 13.6. In the left panel the complete structure is given where the lines of the finite element mesh are displayed. It can be seen that our model corresponds to a Al_2O_3 substrate on which has been deposited a finite film of GaN. The right

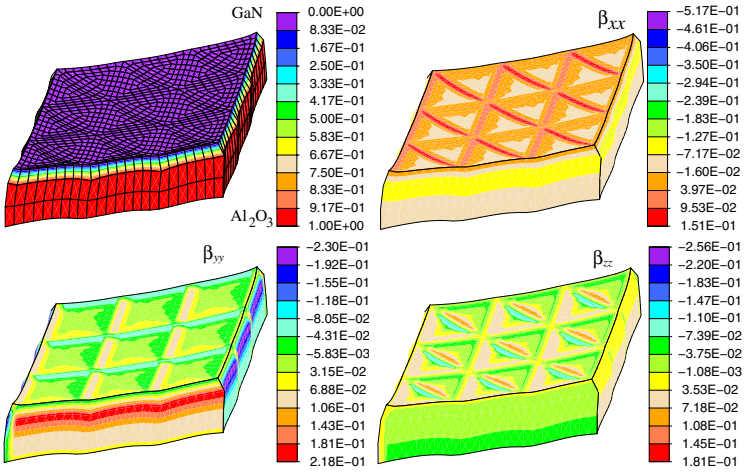

Fig. 13.7 Chemical composition and the lattice distortions $\beta_{xx}, \beta_{yy}, \beta_{zz}$ in the spring-back configuration induced by stress relaxation of the 27-node FE mesh reflecting the global honey-comb structure through a co-set decomposition of the primitive unit-cell described in Section 13.4.1 (*c.f.* figure 13.6).

panel shows the same as the left, but as a slice through the interface region in the [0001] direction revealing the GaN surface and network of three crossing line dislocations *c.f.* figures 13.5b and 13.6c. Residual stresses arising in the interface region are given in figure 13.8. These results indicate that a honeycomb network of misfit dislocations arising from the lattice mismatch between GaN and Al_2O_3 is energetically stable.

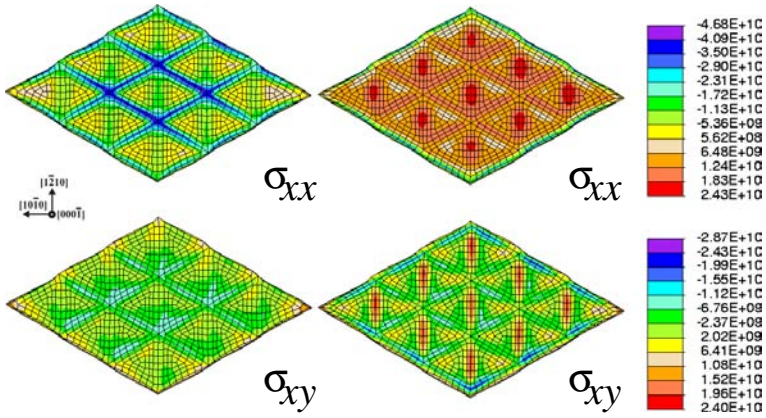

Fig. 13.8 A cross-section through the [0001] direction revealing relaxed honeycomb Cauchy stress field [Pa] on (left) Al_2O_3 and right GaN surface.

13.5 Conclusions

The aim of this paper was to achieve modelling of dislocations by means of the atomistic and continuum models including:

(a) The reconstruction (preprocessing) of the dislocations and stacking faults by means of the use of a modified analytical formulae to input the mixed dislocation into the atomistic model, see (13.7) and Fig. 13.2. The reconstruction of analogical models based on the analysis of the HRTEM image is also discussed, see and Fig. 13.3.
(b) The use of the computer image processing based on GPA as the input data to the FEA of interfacial region, see Fig. 13.4. The modelling takes into account the residual stresses and lattice distortion distribution induced by both: (a) the chemical mismatch of different type crystal lattices (b) misfit dislocations and (c) elastic residual stress/strain field accommodating the remaining mismatch.

The continuum models used in this work have the significant advantage of treating large volumes without utilising millions of atoms in the formalism while providing an understanding of defect interactions. As a realistic example of this we have investigated the strain response affected by misfit dislocations in the heterostructure GaN/Al_2O_3. This was achieved starting from observations of HRTEM images, and through its computer image processing resulting 2D lattice distortion field, reconstruction of missing distortion field in the 3rd direction, and finally by the 3D FE modelling of the misfit dislocation net. The results from our method of modelling have been shown to be consistent with experiment.

The method we have employed here is not limited to a traditional film/substrate system and can be easily extended to include more complex structures; such as for example, sequential multi-layers intersected by treading dislocations. Furthermore the computational process presented here can be used hand-in-hand with other techniques of HRTEM interpretation.

Acknowledgements

This research was carried out in the framework of the European Commission PARSEM project MRTN-CT-2004-005583 additionally subsided by the Ministry of Science and Higher Education (MSHE) in Poland grant 131/6PREU/2005/7 in the period 1 Mar 2006 – 28 Feb 2009. Since 1 Mar 2009 the investigations are continued in the framework of the grant 0634/R/T02/2007/02 founded by MSHE.

References

[1] Béré, A., Serra, A.: Atomic structure of dislocation cores in GaN. Physical Review B 65, 205323 (2002)
[2] Béré, A., Serra, A.: Atomic structure of dislocation cores in GaN. Phys. Rev. B 65(20), 205323 (2002)
[3] de Wit, R.: Theory of dislocations II, continuous and discrete dislocations in anisotropic elasticity. J. Research of Nat. Bur. Stand (USA) — A. Phys. Chem. 77A, 608 (1973)
[4] Dłużewski, P.: Anisotropic hyperelasticity based upon general strain measures. Journal of Elasticity 60(2), 119–129 (2000)
[5] Dłużewski, P., Jurczak, G., Antúnez, H.: Logarithmic measure of strains in finite element modelling of anisotropic deformations of elastic solids. Computer Assisted Mechanics and Engineering Science 10, 69–79 (2003)
[6] Dłużewski, P., Maciejewski, G., Jurczak, G., Kret, S., Laval, J.-Y.: Nonlinear FE analysis of residual stresses induced by misfit dislocations in epitaxial layers. Computational Materials Science 29(3), 379–395 (2004)
[7] Dłużewski, P., Young, T., Dimitrakopoulos, G., Komninou, P.: Continuum and atomistic modelling of the mixed straight dislocation. Int. J. Multiscale Computational Engineering (2009) (accepted for publication)
[8] Fall, C.J., Jones, R., Briddon, P.R., Blumenau, A.T., Frauenheim, T., Heggie, M.I.: Influence of dislocations on electron energy-loss spectra in gallium nitride. Phys. Rev. B 65(24), 245304 (2002)
[9] Hÿtch, M., Putaux, J.-L., Pénisson, J.-M.: Measurement of the displacement field of dislocations to 0.03Å by electron microscopy. Nature 423, 270–273 (2003)
[10] Hÿtch, M.J., Snoeck, E., Kilaas, R.: Quantitative measurement of displacement and strain fields from HTEM micrographs. Ultramicroscopy 74, 131–146 (1998)
[11] Kioseoglou, J., Dimitrakopulos, G., Komninou, P., Kehagias, T., Karakostas, T.: Phys. Status Solidi A 203, 2156 (2006)
[12] Kioseoglou, J., Dimitrakopulos, G.P., Komninou, P., Karakostas, T.: Atomic structures and energies of partial dislocations in wurtzite GaN. Phys. Rev. B 70(3), 035309 (2004)
[13] Kioseoglou, J., Dimitrakopulos, G.P., Komninou, P., Karakostas, T., Aifantis, E.: Dislocation core investigation by geometric phase analysis and the dislocation density tensor. J. Phys. D: Appl. Phys. 41, 035408 (2007)
[14] Komninou, P., Kioseoglou, J., Dimitrakopulos, G., Kehagias, T., Karakostas, T.: Phys. Status Solidi A 202, 2888 (2005)
[15] Kret, S., Dłużewski, P., Dłużewski, P., Laval, J.-Y.: On the measurement of dislocation cores distribution in GaAs/ZnTe/CdTe heterostructure by transmission electron microscopy. Philosophical Magazine A 83, 231–244 (2003)
[16] Kröner, E.: Continuum theory of defects. In: Balian, R., Kleman, M., Poiries, J.-P. (eds.) Physics of Defects, pp. 215–315. North-Holland, Amsterdam (1981)
[17] Lee, S.M., Belkhir, M.A., Zhu, X.Y., Lee, Y.H., Hwang, Y.G., Frauenheim, T.: Electronic structures of gan edge dislocations. Phys. Rev. B 61(23), 16033–16039 (2000)
[18] Leung, K., Wright, A., Stechel, E.: Charge accumulation at a threading edge dislocation in gallium nitride. Applied Physics Letters 74, 2495 (1999)
[19] Love, A.E.H.: Mathematical Theory of Elasticity. Cambridge University Press, Cambridge (1927)
[20] Lymperakis, L.: Ab-Initio Based Multiscale Calculations of Extended Defects in and on Group III – Nitrides. PhD thesis, Department Physik der Fakultät für Naturwissenschaften an der Universität Paderborn (2005)

[21] Lymperakis, L., Neugebauer, J., Albrecht, M., Remmele, T., Strunk, H.P.: Strain induced deep electronic states around threading dislocations in GaN. Phys. Rev. Lett. 93(19), 196401 (2004)
[22] Potin, V., Ruterana, P., Nouet, G., Pond, R.C., Morkoç, H.: Mosaic growth of gan on (0001) sapphire: A high-resolution electron microscopy and crystallographic study of threading dislocations from low-angle to high-angle grain boundaries. Phys. Rev. B 61(8), 5587–5599 (2000)
[23] Read Jr., W.T.: Dislocations in Crystals. McGraw-Hill, London (1953)
[24] Spaepen, F.: Interfaces and stresses in thin films. Acta Materialia 48, 31–42 (2000)
[25] Stadelmann, P.: EMS - A software package for electron diffraction analysis and hrem image simulation in materials science. Ultramicroscopy 21, 131 (1987)
[26] Wright, A., Grossner, U.: The effect of doping and growth stoichiometry on the core structure of a threading edge dislocation in GaN. Applied Physics Letters 73, 2751 (1998)